

THERMAL RADIATION MIXED CONVECTION BOUNDARY-LAYER FLOW IN TIGHTLY COILED CURVED PIPE FOR LARGE RICHARDSON NUMBER

by

Muhammad ASHRAF*, Robina YASMEEN, and Masud AHMAD

Department of Mathematics, Faculty of Science, University of Sargodha, Sargodha, Pakistan

Original scientific paper

<https://doi.org/10.2298/TSCI150805120A>

The characteristics of radiative mixed convection boundary-layer flow generated close to the inner walls of tightly coiled curved pipe for full range of Richardson number is investigated. In order to find numerical solutions the governing coupled, non-linear PDE are transformed into convenient form for integration by using primitive variable formulation. From this transformation the terms highest powers of Dean number are retained into boundary-layer form and then solved numerically by using finite difference method. Expressions for the axial and transverse components of skin friction, heat transfer coefficient, and flux thicknesses for various values of Richardson number, λ , angle, α , curvature of the pipe, Planck number, R_ϕ , and Prandtl number are obtained and given graphically.

Key words: *coiled curved pipe, mixed convection, thermal radiation, curvature, Dean number, finite difference method*

Introduction

The idea of boundary-layer flow in coiled curved pipe has given much attention due to its applications in blood flow in human arterial system. The largest vessel in this system, the aorta, is highly curved. In the case of heat transfer the secondary motions can be expected to enhance heat exchange between the fluid and its surroundings, so the knowledge of the magnitude of this effect is important in designing heat exchangers. The flow in curved pipes is characterized by Dean number ($D = \delta^{1/2}$), and curvature (tightly coiled pipe in which $0 < \delta < 1$). Dean number is the measure of magnitude of the secondary flow and, δ , the curvature of the pipe, measures the variation of centrifugal force on the cross-section. History of boundary-layer flow in coiled tubes is too long and cannot be discussed in a small scale, yet we present a detail review of past few decades. Cuming [1] studied the secondary flow in curved pipes and presented the Navier-Stokes equation for the flow field in power series of the curvature of the pipe. In designing a hypersonic low-density wind tunnel the main problem faced is to devise a pumping system that can handle high volume flows at the tunnel exit. This flow is associated with boundary-layer generating at the nozzle entrance for which the nozzle diameter must be checked. Bottorff and Rogers [2] presented theoretical and experimental results on the reduction of boundary-layer thickness at low density nozzles by wall suction, wall cooling and their combined effects. Srivastava and Laxman [3] studied the heat transfer in curved annulus for hydrodynamically and thermally fully developed laminar flow by method of series expansion. Yao

* Corresponding author, e-mail: mashraf682003@yahoo.com

[4] studied in detail the laminar flow convective heat transfer in curved pipes, heated, and unheated straight pipes. Secondary flow occurs whenever the flow is in curved pipes which is why the analysis of fluid-flow in curved conduits is rather difficult than in straight paths. Berger [5] discussed the fluid-flow in curved pipes for developing and fully developed flow for both steady and unsteady flows in rigid infinitely coiled pipes, finite bends and most importantly the thermal effects on the flow. Narasimaha *et al.* [6] analyzed the phenomenon of steady heat transfer enhancement in a steady laminar flow through a tube using two different coils.

Coiled pipes and curved tubes are used as a passive technique for heat exchanges due to their compact structure and high heat transfer coefficient. Using this method Paisran and Somchai [7] presented a detailed review on single-phase and two-phase heat transfer and flow characteristics in curved tubes. Petrakis *et al.* [8] presented the numerical solutions for a viscous incompressible fluid in a curved annular duct with the Dean number up to 8000. Castiglia *et al.* [9] studied time-dependent numerical simulation results for the flow in toroidal coordinates with heat transfer of a constant property fluid with $Pr = 1$. Chauhan and Kumar [10] assumed a gray fluid which can absorb and emit radiation and analyzed theoretically a fully developed mixed convection viscous fluid flowing between two infinite vertical parallel plane walls in the presence of radiation and viscous dissipation effects. Mahmoodi [11] numerically investigated the mixed convection fluid flow and heat transfer in lid-driven rectangular enclosures filled with the Al_2O_3 -water nanofluid by keeping all the walls of the enclosure at a constant cold temperature.

Helical coils have been long and widely used as heat exchangers in power, petrochemical, HVAC, chemical, and many other industrial processes. The reason is because they have a better heat transfer rate than straight tubes due to the formation of a secondary flow along with a primary flow in the curved tubes. Considering this fact Elazym *et al.* [12] introduced the concept of helical cone coils and analyzed the heat transfer rates in them compared with the simple helical coils. The flow over cylinders is considered axi-symmetric instead of 2-D when the radius of cylinder is of the same order as the boundary-layer thickness for which the governing equations include transverse curvature term. To describe this phenomenon in detail Poplay *et al.* [13] presented the effects of thermal radiation on axi-symmetric laminar boundary-layer flow of a viscous incompressible fluid along a stretching cylinder using Rosseland approximation.

In keeping view the literature survey, we investigate the boundary-layer mixed convection flow of viscous, incompressible, optically dense grey fluid generated at the entrance of the curved pipe for large values of Richardson number.

Formulation of mathematical model and co-ordinate system

Here we consider radiative mixed convection boundary-layer flow of viscous, incompressible, optically dense grey fluid. The velocity components in the (r, a, z) -directions are taken, respectively.

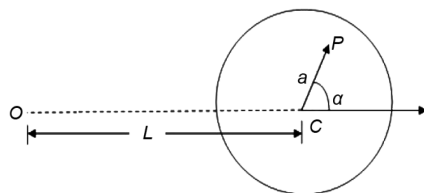


Figure 1. Section of the coiled pipe

Let a circle Γ with centre O and radius L , and C is the circular cross-section of the pipe with radius a coiled in the circle Γ (fig. 1). Let $\delta = a/L$ be the curvature of the pipe. By following Stewartson *et al.* [14] and Berger *et al.* [5] with the inclusion of energy equation for radiative heat transfer, the boundary-layer equations are given:

$$\frac{\partial u}{\partial r} + \frac{u}{r} \left(\frac{1+2\delta r \cos \alpha}{1+\delta r \cos \alpha} \right) + \frac{1}{r} \frac{\partial v}{\partial \alpha} - \frac{\delta v \sin \alpha}{1+\delta r \cos \alpha} + \frac{1}{1+\delta r \cos \alpha} \frac{\partial w}{\partial z} = 0 \quad (1a)$$

$$\begin{aligned} & u \frac{\partial u}{\partial r} + \frac{v}{r} \frac{\partial u}{\partial \alpha} + \frac{w}{1+\delta r \cos \alpha} \frac{\partial u}{\partial z} - \frac{v^2}{r} - \frac{w^2 \cos \alpha}{1+\delta r \cos \alpha} = -\frac{1}{\delta} \frac{\partial p}{\partial r} \\ & - \frac{\nu \text{Re}^{1/2}}{aD} \left\{ \left(\frac{1}{r} \frac{\partial}{\partial \alpha} - \frac{\delta \sin \alpha}{1+\delta r \cos \alpha} \right) \left(\frac{\partial v}{\partial r} + \frac{v}{r} - \frac{1}{r} \frac{\partial u}{\partial \alpha} \right) \right. \\ & \left. - \frac{\delta}{(1+\delta r \cos \alpha)^2} \frac{\partial^2 u}{\partial z^2} + \frac{1}{1+\delta r \cos \alpha} \left(\frac{\partial^2 w}{\partial r \partial z} + \frac{\delta \cos \alpha}{1+\delta r \cos \alpha} \frac{\partial w}{\partial z} \right) \right\} \end{aligned} \quad (1b)$$

$$\begin{aligned} & u \frac{\partial v}{\partial r} + \frac{v}{r} \frac{\partial v}{\partial \alpha} + \frac{w}{1+\delta r \cos \alpha} \frac{\partial v}{\partial z} + \frac{uv}{r} + \frac{w^2 \sin \alpha}{1+\delta r \cos \alpha} = -\frac{1}{r\delta} \frac{\partial p}{\partial \alpha} + \\ & + \frac{\nu \text{Re}^{1/2}}{aD} \left\{ \left(\frac{\partial}{\partial r} + \frac{\delta \cos \alpha}{1+\delta r \cos \alpha} \right) \left(\frac{\partial v}{\partial r} + \frac{v}{r} - \frac{1}{r} \frac{\partial u}{\partial \alpha} \right) \right. \\ & \left. + \frac{\delta}{(1+\delta r \cos \alpha)^2} \frac{\partial^2 v}{\partial z^2} - \frac{1}{1+\delta r \cos \alpha} \left(\frac{1}{r} \frac{\partial^2 w}{\partial \alpha \partial z} + \frac{\delta \sin \alpha}{1+\delta r \cos \alpha} \frac{\partial w}{\partial z} \right) \right\} + \\ & + aD^{1/2} \text{Re}^{-1} g\beta(T - T_\infty) \end{aligned} \quad (1c)$$

$$\begin{aligned} & u \frac{\partial w}{\partial r} + \frac{\delta u w \cos \alpha}{1+\delta r \cos \alpha} + \frac{v}{r} \frac{\partial w}{\partial \alpha} - \frac{\delta \sin \alpha}{1+\delta r \cos \alpha} v w + \frac{w}{1+\delta r \cos \alpha} \frac{\partial w}{\partial z} = -\frac{1}{1+\delta r \cos \alpha} \frac{\partial p}{\partial z} + \\ & + \frac{\nu \text{Re}^{1/2}}{aD} \left\{ \left(\frac{\partial}{\partial r} + \frac{1}{r} \right) \left(\frac{\partial w}{\partial r} + \frac{\delta w \cos \alpha}{1+\delta r \cos \alpha} - \frac{\delta}{1+\delta r \cos \alpha} \frac{\partial u}{\partial z} \right) \right. \\ & \left. + \frac{1}{r^2} \frac{\partial^2 w}{\partial \alpha^2} - \frac{1}{r} \frac{\partial}{\partial \alpha} \left(\frac{\delta w \sin \alpha}{1+\delta r \cos \alpha} \right) - \frac{1}{r} \frac{\partial}{\partial \alpha} \left(\frac{\delta}{1+\delta r \cos \alpha} \frac{\partial v}{\partial z} \right) \right\} + \\ & + aD^{1/2} \text{Re}^{-1} g\beta(T - T_\infty) \end{aligned} \quad (1d)$$

$$\frac{\rho c_p}{1+\delta \cos \alpha} \left(u \frac{\partial T}{\partial r} + \frac{v}{r} \frac{\partial T}{\partial \alpha} + \frac{w}{1+\delta \cos \alpha} \frac{\partial T}{\partial z} \right) = \frac{1}{arD} \frac{\partial}{\partial r} \left\{ \left[\frac{16\sigma T^3}{3(a+\sigma_s)} + k \right] r \frac{\partial T}{\partial r} \right\} \quad (1e)$$

The appropriate boundary conditions applied to the present problem are:

$$u = v = w = 0, \quad T = T_w \quad \text{at} \quad r = 1, \quad z > 0, \quad u \rightarrow u_\infty, \quad T \rightarrow T_\infty \quad \text{as} \quad r \rightarrow \infty \quad (2)$$

Group of transformations

To solve eq. (1) subject to the boundary conditions (2), we extend the transformations introduced by Stewartson *et al.* [14] valid with in a distance $O(D^{-1/2})$ into primitive variable formulation of the following form:

$$\left. \begin{aligned} Y &= (1-r)D^{1/2}, \quad u = \frac{-V}{a} \operatorname{Re}^{1/2} D^{-1/2} U(Y, \alpha, z), \quad v = \frac{\nu \operatorname{Re}^{1/2} V(Y, \alpha, z)}{a(1+\delta \cos \alpha)}, \\ w &= \frac{\nu \operatorname{Re}^{1/2} W(Y, \alpha, z)}{a(1+\delta \cos \alpha)}, \quad p = \frac{\nu^2 \operatorname{Re} P(Y, \alpha, z)}{2a^2(1+\delta \cos \alpha)^2}, \quad \theta(Y, \alpha, z) = D^{1/2} \left(\frac{T - T_\infty}{T_w - T_\infty} \right), \\ \theta_w &= \frac{T_w}{T_\infty}, \quad \operatorname{Re} = \frac{W_o a}{\nu}, \quad \operatorname{R}_d = \frac{4\sigma T_\infty^3}{\kappa(a + \sigma_s)} \end{aligned} \right\} \quad (3)$$

where Y is the primitive variable, D – the Dean number, δ – the curvature of the pipe, Re – the Reynolds number, ν – the kinematics viscosity, θ – the dimensionless temperature coefficient, θ_w – the surface temperature, and R_d – the Planck number.

To examine the boundary-layer behavior valid within a distance $O(D^{-1/2})$ of the wall we use eq. (3) in eq. (1), and retaining only highest powers of D , we get the set of transformed boundary-layer equations:

$$\frac{\partial U}{\partial Y} + \frac{1}{(1+\delta \cos \alpha)} \frac{\partial V}{\partial \alpha} + \frac{1}{(1+\delta \cos \alpha)^2} \frac{\partial W}{\partial z} = 0 \quad (4a)$$

$$\begin{aligned} U \frac{\partial V}{\partial Y} + \frac{V}{(1+\delta \cos \alpha)} \frac{\partial V}{\partial \alpha} + \frac{W}{(1+\delta \cos \alpha)^2} \frac{\partial V}{\partial z} + \frac{\sin \alpha}{(1+\delta \cos \alpha)^2} (\delta V^2 + W^2 - 1) = \\ = \frac{\partial^2 V}{\partial Y^2} + \lambda(1+\delta \cos \alpha)\theta \end{aligned} \quad (4b)$$

$$U \frac{\partial W}{\partial Y} + \frac{V}{(1+\delta \cos \alpha)} \frac{\partial W}{\partial \alpha} + \frac{W}{(1+\delta \cos \alpha)^2} \frac{\partial W}{\partial z} = \frac{\partial^2 W}{\partial Y^2} + \lambda(1+\delta \cos \alpha)\theta \quad (4c)$$

$$\frac{1}{(1+\delta \cos \alpha)} \left[U \frac{\partial \theta}{\partial Y} + \frac{V}{(1+\delta \cos \alpha)} \frac{\partial \theta}{\partial \alpha} + \frac{W}{(1+\delta \cos \alpha)^2} \frac{\partial \theta}{\partial z} \right] = \frac{1}{\operatorname{Pr}} r_1 \frac{\partial^2 \theta}{\partial Y^2} \quad (4d)$$

where $r_1 = 4/3\operatorname{R}_d + 1$.

The transformed boundary conditions are given:

$$U = V = W = 0, \quad \theta = 1 \quad \text{at} \quad Y = 0, \quad V \rightarrow 0, \quad W \rightarrow 1, \quad \theta \rightarrow 0 \quad \text{as} \quad Y \rightarrow \infty \quad (5)$$

Method of solution

The numerical solution of transformed equations subject to the boundary conditions is carried out using finite difference method. As the velocity components become independent of z , as $z \rightarrow \infty$ therefore we present our numerical solution by neglecting $\partial/\partial Z = 0$ in eq. (4) and solving the resulting 3-D parabolic equations. We will discretize eq. (4) with boundary conditions (5) using backward difference for α -direction and central difference for Y -direction. We get the system of tri-diagonal algebraic equations. We solve this tri-diagonal system of equation by using Gaussian elimination technique. The discretized form of each term of eq. (4) along with boundary conditions (5) is:

$$\begin{aligned} A_1 V_{i+1,j} + B_1 V_{i,j} + C_1 V_{i-1,j} &= D_1 \\ A_2 W_{i+1,j} + B_2 W_{i,j} + C_2 W_{i-1,j} &= D_2 \\ A_3 \theta_{i+1,j} + B_3 \theta_{i,j} + C_3 \theta_{i-1,j} &= D_3 \end{aligned} \quad (6)$$

The velocity can be calculated directly using equation of continuity (4a):

$$V_{i,j} = V_{i,j+1} + \frac{(1 + \delta \cos \alpha) \Delta \alpha}{2 \Delta Y} (U_{i-1,j} - U_{i+1,j}) \quad (7)$$

The computation is started at $z = 0.0$ and marches down implicitly. Here, we have taken step size $\Delta z = 0.005$ and $\Delta Y = 0.01$ for i and j grid points and the maximum grid points 150 in the following computation with tolerance $\varepsilon = 0.0001$ for the convergence of the obtained numerical results. Further, we calculate the skin friction for transverse, axial direction and rate of heat transfer with the help of following mathematical expression:

$$\tau_{\text{trans}} = \mu \left(\frac{\partial V}{\partial Y} \right)_{Y=0}, \quad \tau_{\text{axial}} = \mu \left(\frac{\partial W}{\partial Y} \right)_{Y=0}, \quad \text{Nu} = \left(1 + \frac{4}{3} \text{R}_d \theta_w^3 \right) \left(\frac{\partial \theta}{\partial Y} \right)_{Y=0} \quad (8)$$

Results and discussions

Here we discuss the behavior of chief physical quantities such as skin friction and rate heat transfer affected by different dimensionless parameters such as Prandtl number, Richardson number, λ , Planck number, R_d , angle, α , and curvature, $\delta = a/L$.

Effects of different parameters on skin friction and rate of heat transfer

The flow of the fluid is along z -axis down the pipe that is why the variation of parameters is taken along z -axis. Figure 2 represents the variation of skin friction and rate of heat transfer for various values of α . From these figures it is noted that the maximum skin friction along transverse direction is at $\alpha = 0$ and minimum at $\alpha = 60^\circ$, similarly the axial component of skin friction is maximum at $\alpha = 0^\circ$ and shown down drag at $\alpha = 60^\circ$ exact at the surface and attains its asymptotic behavior at $z = 0.2$ for the same angle. Figure 2(c) predicts the behavior of rate of heat transfer, from this figure maximum rate of heat transfer is observed at $\alpha = 60^\circ$ and minimum at $\alpha = 0^\circ, 120^\circ$. Figures 3(a)-3(c) show the effects of dif-

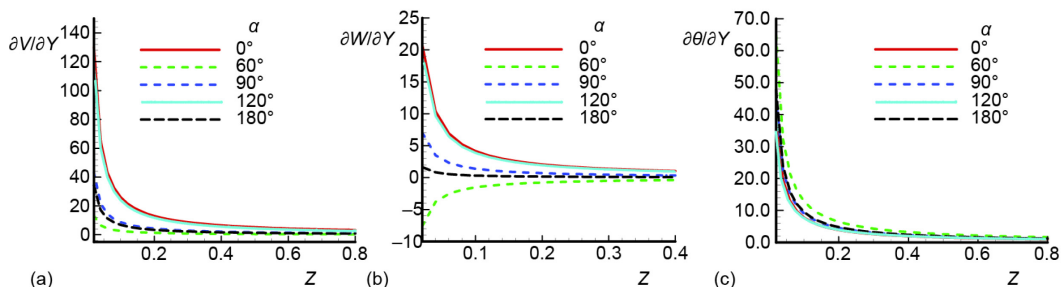


Figure 2. (a) Variation of transverse skin friction with z for various α , (b) variation of axial component of skin friction with z for various α , (c) variation of rate of heat transfer with z for various values of α ; when $\text{Pr} = 7.0$, $\delta = 0.9$, $\text{Gr} = 1000.0$, $\text{R}_d = 0.1$, and $\theta_w = 0.3$ (for color image see journal web site)

ferent values of Richardson number on skin friction components and rate of heat transfer. From these figures it is concluded that the transverse component of skin friction is maximum for large value of Richardson number $\lambda = 1000.0$ and is minimum, and same for $\lambda = 0.1, 1.0, 10.0, 100.0$. The totally down drag is noted for the case of axial component of skin friction and behavior is asymptotic for $z = 1.5$ as in fig. 3(b). It is also noted from fig. 3(c) that the rate of heat transfer is maximum for large value of $\lambda = 1000.0$ and is decreased uniformly for $\lambda = 0.1, 1.0, 10.0$ and 100.0 . Figures 4(a) and 4(b) show typical contribution of curvature of pipe, δ , on transverse, axial components of skin friction, and rate of heat transfer. From these figures we can observe that for small values of curvature $\delta = 0.01, 0.08$ the transverse and axial components of skin friction maximum and for large value of $\delta = 0.9$ both quantities are decreased drastically. The rate of heat transfer is also remarkable for very small value of $\delta = 0.01$ and there is no change seen for other values of curvature δ .

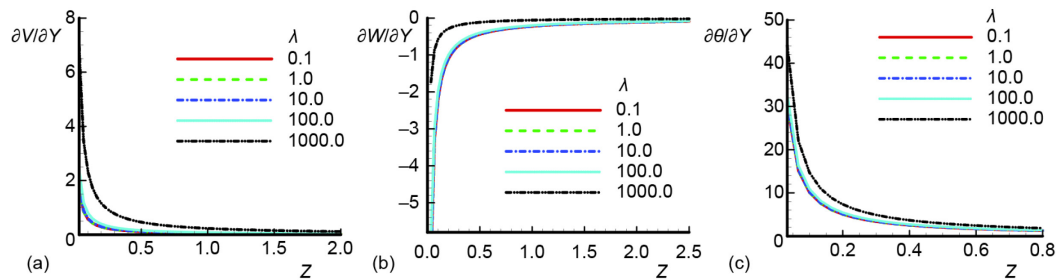


Figure 3. (a) Variation of transverse skin friction with z for various λ , (b) variation of axial component of skin friction with z for various λ , (c) variation rate of heat transfer with z for various values of λ ; when $Pr = 7.0$, $\alpha = 180^\circ$, $\delta = 0.9$, $R_d = 0.1$, and $\theta_w = 0.3$ (for color image see journal web site)

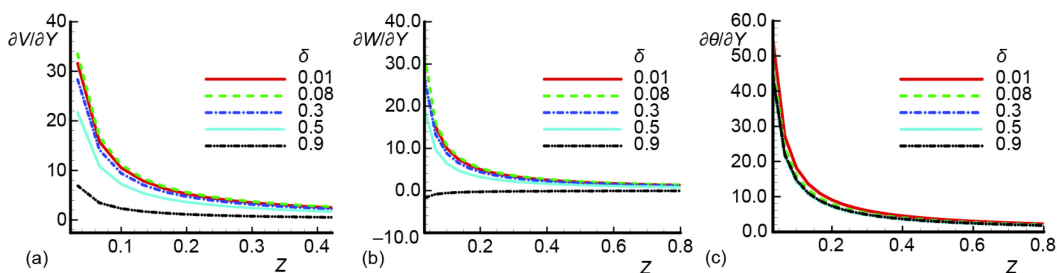


Figure 4. (a) Variation of transverse skin friction, (b) variation of axial component of skin friction, (c) variation of rate of heat transfer with z for various values of δ for $Pr = 7.0$, $\alpha = 180^\circ$, $Gr = 1000.0$, $R_d = 0.1$, and $\theta_w = 0.3$ (for color image see journal web site)

The behavior of transverse, axial components of skin friction, and rate of heat transfer is illustrated in figs. 5(a)-5(c) for various values of Planck number. It can be seen that the transverse and axial components of skin friction are significantly increased but the rate of heat transfer is decreased with the increase of $R_d = 50.0$. Figs. 6(a)-6(c) reveal the effect of different values of Prandtl number on transverse, axial components of skin friction and rate of heat transfer. It is evident that the transverse and axial components of skin frictions are decreased while the rate of heat transfer is increased. The observation is consistent with the underlying physical mechanism that the increase in Prandtl number increases the viscosity of the fluid which strong the molecular interaction force of the fluid that increase the rate of heat transfer.

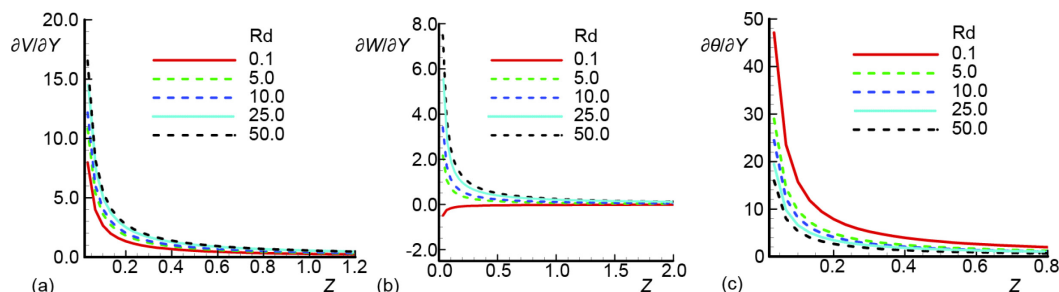


Figure 5. (a) Variation of transverse skin friction, (b) variation of axial component of skin friction, (c) variation of rate of heat transfer with z for various values of R_d ; $Pr = 7.0$, $\alpha = 180^\circ$, $Gr = 1000.0$, $\theta_w = 0.3$, and $\delta = 0.9$ (for color image see journal web site)

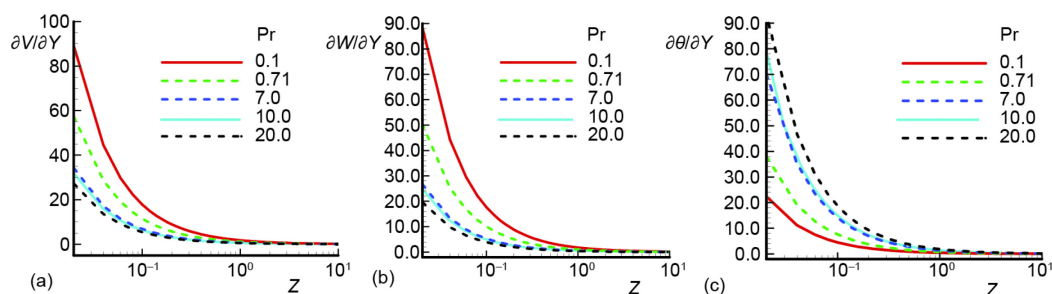


Figure 6. (a) Variation of transverse skin friction, (b) variation of axial component of skin friction, (c) variation of rate of heat transfer with z for various values of Prandtl number; when $\alpha = 180^\circ$, $\delta = 0.9$, $R_d = 0.1$, $\theta_w = 0.3$, and $Gr = 1000.0$ (for color image see journal web site)

Effects of different parameters on velocity and temperature profile

In practical engineering applications the phenomena of transverse and axial components of velocity along with temperature distribution in the fluid-flow domain is very important. With this understanding in this section we present the numerical solutions of these profiles graphically.

Results of the numerical study are summarized in figs. 7(a)-7(c), which exhibit the variation of α and the behavior appears as the transverse component of velocity is increased

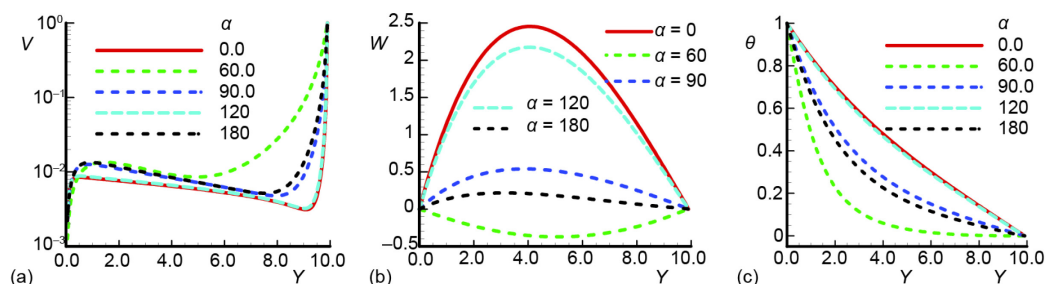


Figure 7. (a) Transverse component of velocity profile V , (b) axial component of velocity profile W , (c) temperature distribution θ for different values of α against Y ; for $Pr = 7.0$, $\delta = 0.9$, $Gr = 100.0$, $R_d = 0.1$, and $\theta_w = 0.3$ (for color image see journal web site)

for $\alpha = 60^\circ$ and is decreased for $\alpha = 0^\circ, 120^\circ$, axial component of velocity is maximum at $\alpha = 0^\circ$ and minimum for $\alpha = 60^\circ$ and temperature profile attains its maximum value for $\alpha = 0^\circ, 120^\circ$ but drastically attains its minimum position for $\alpha = 60^\circ$. It happens because for $\alpha = \pi$ the cross flow boundary-layer behaves like subboundary-layer below the axial flow. Velocity and temperature profile for different value of curvature δ is described in figs. 8(a)-8(c). Inspection of the solution shows that the transverse component of velocity is increased for $\delta = 0.9$ and decreases for $\delta = 0.1$, axial component of velocity is increased for $\delta = 0.1$ and decreases for $\delta = 0.9$ which is inverse of the transverse component of velocity and temperature distribution is maximum for $\delta = 0.1$ and becomes slow at maximum curvature of pipe $\delta = 0.9$. This behavior can be termed as the collision phenomenon is an important feature of the entry boundary-layer for tightly coiled curved pipe ($0 < \delta < 1$). In figs. 9(a)-9(c) the effect of the velocity and temperature for different values of Planck number are shown graphically. It is observed that the transverse component of velocity increases with increasing Planck number and the axial component of velocity increases in the upstream region of the coiled curved pipe. It is interesting to note that an increase in the Planck number leads to increase temperature profile of the flow field. Increase in the value of Planck number have a tendency to slow down the movement of the fluid at the middle portion of the tightly coiled curve pipe.

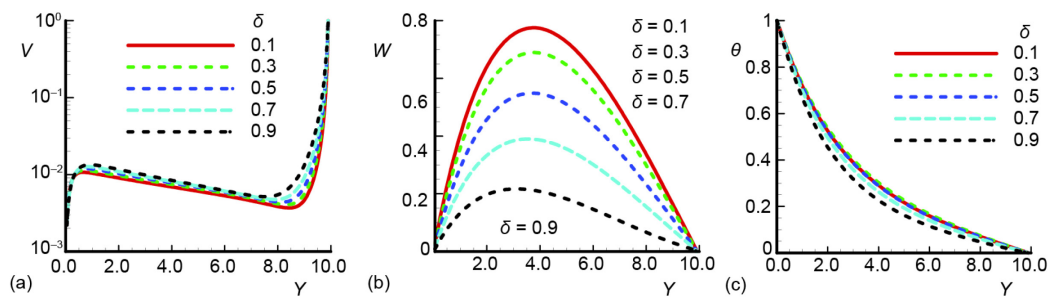


Figure 8. (a) Transverse component of velocity profile V , (b) axial component of velocity profile W , (c) temperature distribution θ for various values of δ when $Pr = 7.0$, $\alpha = 180^\circ$, $Gr = 100.0$, $R_d = 0.1$, and $\theta_w = 0.3$ (for color image see journal web site)

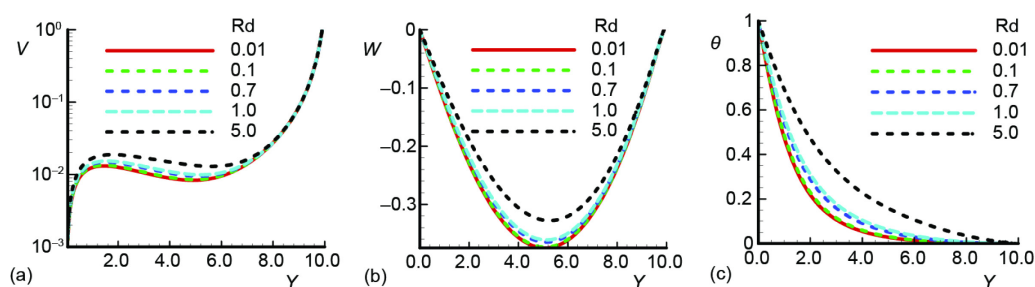


Figure 9. (a) Transverse component of velocity profile V , (b) axial component of velocity profile W , (c) temperature distribution θ for various values of R_d when $Pr = 7.0$, $\alpha = 60^\circ$, $\delta = 0.9$, $Gr = 100.0$, and $\theta_w = 0.3$

Conclusions

The previously described calculation are intended to demonstrate the large influence of Richardson number combined with other parameters involved in the fluid-flow domain in

the presence of thermal radiation. The range of different parameters involved in fluid-flow model for which the solution is reliable. Derived in terms of transverse and axial component of skin friction and velocity profile. The same attempt has been made for the case of heat transfer and temperature distribution. In the problem of coiled curved pipe the behavior of aforementioned quantities for different range of parameter is given as follows.

- The significance and role of angle α in coiled curved pipe has been brought out in quantitative ways and it is clear that the transverse and axial components of skin friction are strong at $\alpha = 0^\circ$ and the rate of heat transfer is noted maximum at $\alpha = 60^\circ$. For the case Richardson number the maximum transverse skin friction is occurred for $\lambda = 1000.0$ and the down drag is noted for the case of axial component of skin friction, while the rate of heat transfer is increased with the increase of Richardson number which is quite naturally. It is also shown that with the increase of curvature (degree of bent of coiled curved pipe) the transverse, axial component of skin friction along with rate of heat transfer is decreased unanimously. The variation of Planck number is found to have significant effect on transverse, axial component of skin friction and rate of heat transfer. Graphical results for different values of Prandtl number are presented and it is found that transverse, axial components of skin friction are decreased while the rate of heat transfer is increased.
- The present simulation has demonstrated that the transverse, axial component of velocity profile are maximum and minimum for angle $\alpha = 60^\circ$, respectively, and temperature profile decreases for the same angle. With the increase of curvature, δ , of the pipe the transverse component of velocity is increased, axial component of velocity and temperature distribution, θ , is decreased. It is found that the transverse component of velocity is increased and axial component of velocity profile is negative and developed with the increase of Planck number on the other hand temperature distribution is increased which is truth with the sense that thermal radiation is included in the energy equation to enhance the temperature of the system under consideration.

Nomenclature

a	– radius of the circular cross-section of pipe, [m]
D	– Dean number ($=\sqrt{\delta} Re$), [–]
g	– acceleration due to gravity, [ms^{-2}]
Gr	– Grashoff number ($=g\beta(T_w - T_\infty)L^3/4\nu$)
Pr	– Prandtl number ($=\nu/\alpha$), [–]
R_d	– Planck number
r	– radial direction, [m]
T	– temperature of the fluid, [K]
T_∞	– ambient fluid temperature, [K]
T_w	– surface temperature, [K]
z	– axial direction, [m]

Greek symbols

β	– volumetric expansion coefficient, [K^{-1}]
δ	– curvature of the pipe ($=a/L$), [–]
θ	– dimensionless temperature function, [–]
κ	– thermal conductivity
λ	– Richardson number ($GrRe^{-2}$), [–]
ν	– kinematic viscosity of fluid, [m^2s^{-1}]
ρ	– fluid density, [kgm^{-3}]
σ	– Stefan-Boltzman constant
σ_s	– scattering coefficient
τ_{axial}	– transient axial stress, [–]
τ_{trans}	– transient shear stress, [–]

References

- [1] Cumming, H. G., The Secondary Flow in Curved Pipes, Report No. 2880, Aeronautical Research Council, London, 1952
- [2] Bootorff, M. R., Rogers, K. W., Theoretical and Experimental Investigation of Boundary Layer Control in Low-Density Nozzles by Wall Suction and Cooling, NASA Technical Memorandum X-53008, University of Southern California, Los Angeles, Cal., USA, 1964
- [3] Srivastava, R. S., Laxman, D., Heat Transfer Effects for a Laminar Flow in a Curved Annulus, *F. C. Auluck, F. N. A.*, 5 (1972), 8, pp. 758-773

- [4] Yao, L. S., Entry Flow in Heated Tubes, Report No. 2111, Defense Advanced Research Projects Agency, Arlington, Va., USA, 1977
- [5] Berger, S. A., et al., Flow in Curved Pipes, *Ann. Rev. Fluid Mech.*, 15 (1983), Jan., pp. 461-512
- [6] Narasimha, A., et al., Analysis of Heat Transfer Enhancement in Coiled Tube Heat Exchangers, *Heat and Mass Transfer*, 44 (2001), 17, pp. 3189-3199
- [7] Paisran, N., Somchai, W., A Review of Flow and Heat Transfer Characteristics in Curved Tubes, *Renewable and Sustainable Energy Reviews*, 10 (2006), 5, pp. 463-490
- [8] Petrakis, M. A., et al., Steady Flow in a Curved Pipe with Circular Cross-Section, *The Open Fuels and Energy Science Journal*, 2 (2009), May, pp. 20-26
- [9] Castiglia, F., et al., Modeling Flow and Heat Transfer in Helically Coiled Pipes, Cirten-Unipa RL-1205, University of Palermo, Palermo, Italy, 2010
- [10] Chauhan, D. S., Kumar, V., Radiation Effects on Mixed Convection Flow and Viscous Heating in a Vertical Channel Partially Filled with a Porous Medium, *Tamkang J. Science and Engineering*, 14 (2011), 2, pp. 97-106
- [11] Mahmoodi, M., Mixed Convection Inside Nano-Fluid Filled Rectangular Enclosures with Moving Bottom Wall, *Thermal Science*, 15 (2011), 3, pp. 889-903
- [12] Elazym, M. A., et al., Computational Analysis for the Effect of the Taper Angle and Helical Pitch on the Heat Transfer Characteristics of the Helical Cone Coils, *The Archive of Mechanical Engineering*, 59 (2012), 3, pp. 361-375
- [13] Poplay, V., et al., Analysis of Laminar Boundary Layer Flow along a Stretching Cylinder in the Presence of Thermal Radiation, *WSEAS Trans. Fluid Mech.*, 8 (2013), 4, pp. 159-164
- [14] Stewartson, K., et al., A Boundary Layer Collision in a Curved Duct, *Q. J. Mech. appl. Math.*, 33 (1980), 1, pp. 59-75